TÜBİTAK

Turkish Journal of Physics

http://journals.tubitak.gov.tr/physics/

Research Article

Turk J Phys
(2019) 43: 26 – 36

doi:10.3906/fiz-1804-9

Effect of left-handed materials in surface plasmon excitation and propagation length

Arif Engin ÇETİN*
İzmir Biomedicine and Genome Center, İzmir, Turkey

Received: 13.04.2018 • **Accepted/Published Online:** 02.11.2018 • **Final Version:** 22.02.2019

Abstract: We investigated the dispersion relation of surface plasmons (SPs) excited in a medium comprised of a left-handed material (LHM) layer. We investigated different light polarizations in SP excitation along an LHM-metal interface. We studied SP excitation through a classical Kretschmann geometry, employing an LHM interlayer between a dielectric and a metal layer. Using this three-layer configuration, we investigated the effect of LHM medium on characterizing SP propagation length, which is directly related to the energy of the surface waves.

Key words: Surface plasmons, dispersion relation, left-handed materials, Kretschmann geometry

1. Introduction

Materials with simultaneous negative permeability and permeability, namely left-handed materials (LHMs), were first introduced by Pendry et al. [1]. The experimental demonstration of LHM systems, utilizing split ring resonators or metallic wires, was demonstrated by Shelby et al. [2]. These artificial materials have been proposed for a variety of applications, such as sensing devices [3], antennas [4], and optical communications [5,6]. SPs have received significant attention due to their extraordinary optical properties [7]. SPs are the surface waves that propagate along an interface between a dielectric and a metal layer (i.e. propagating SPs) or get localized around metallic features (i.e. localized SPs), and their energy dissipates as they propagate along this interface [8,9]. SP excitation through different interfaces has been investigated to employ their unique far- and nearfield properties [10–15]. Recently, LHMs have been also offered to employ in the excitation of SPs [16–18]. Excitation of these unique surface waves through LHM media could open up new routes to new applications.

In this paper, we investigated the dispersion relation of SPs excited through an interface between an LHM medium and a metal layer. We readdressed the polarization effect on SP excitation in LHM media and showed the insufficiency of transverse electric (TE)-polarized light to excite SPs by using Maxwell's equations. We modeled a Kretschmann geometry consisting of an LHM interlayer between a dielectric and a metal layer, and performed finite element method (FEM) simulations and employed generalized pencil of function (GPOF) method to investigate SP excitation in this geometry. Finally, we theoretically studied the effect of LHMs on SP energy dissipation rate, which is directly related to SP propagation length. We showed that, thanks to the presence of LHM medium, SPs can propagate longer distances, which could open up a new route to photonic devices compensating material losses. This outcome could be very beneficial for, e.g., low-loss

*Correspondence: arifengin.cetin@ibg.edu.tr

optical communication, plasmonic platforms allowing strong light transmission or reflection in bio-detection or spectroscopy applications, or efficient light conversion in photovoltaic applications.

2. Materials and methods

SP dispersion relation for a two-layer system, consisting of a dielectric medium and a metal layer, is $k_{sp} = k_0\sqrt{(\varepsilon_d\varepsilon_m)}/(\varepsilon_d+\varepsilon_m)$, where k_{sp} and k_0 are the SP and free-space photon wavenumbers, ε_d and ε_m are the dielectric constants of dielectric and metal layers. Figure 1a shows the FEM simulation (COMSOL Multiphysics) of a dipole source located along an interface between a dielectric and a metal layer. SP momentum is greater than that of free-space photon, i.e. light from free space cannot excite SPs. Therefore, for a system consisting of a flat metal film, an evanescent incident source is required to excite SPs. Since dipoles are the source of both propagating and decaying (evanescent) electromagnetic fields, they are able to excite SPs at the metal surface. For the system shown in Figure 1a, the component of the electromagnetic field generated by the dipole at the metal surface (along x-axis) can be approximated as $\Upsilon e^{-jk_x x}/\sqrt{x}$, where Υ is the amplitude of the field. In order to determine the component of the wavevector at the metal surface (k_x), we used the GPOF method (see Supporting Information text for details), where we can approximate field functions as sum of complex exponentials [19–21]. Here, we first multiplied the field data by $\sqrt{x}$ in order to have only a sum of exponentials, i.e. $\Upsilon e^{-ik_x x}$ and then, fitted the data to exponentials to find the wavevector, k_x. In Figure 1b, we showed the tangential component of the wavevector, k_x, the wave component which propagates at the metal surface. The figure demonstrates that the GPOF method successfully extracts the SP wavenumber from the data of the steady-state simulation, which consist of sum of variety of electromagnetic fields. This result shows that with distance from the dipole, the wavevector (red dots) converges to SP wavevector (grey line), which shows that at the locations far from the dipole source, SPs are the dominant electromagnetic fields.

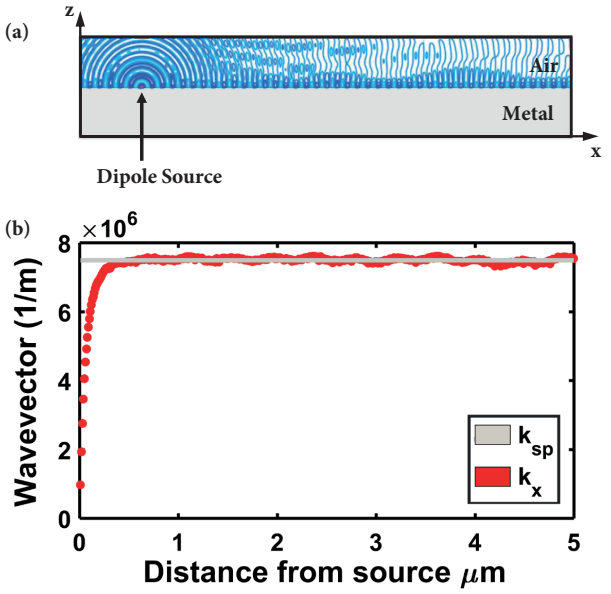

Figure 1. (a) FEM simulation of a dipole locating at a metal surface. (b) Tangential component of the wavevector extracted by the GPOF method from the FEM simulation (red dots) and the SP wavevector (grey line) calculated by the SP dispersion relation. Simulation is performed at $852\,nm$, where $\varepsilon_m = -3322 - j117$ (silver) and $\varepsilon_m = 1$.

3. Results

3.1. SP dispersion relation for LHM–metal interface

LHMs are materials that possess simultaneous negative permittivity (ε) and permeability (μ) [22]. In this section, we investigated the excitation of SPs for a system consisting of an LHM medium on top of a metal layer as illustrated in Figure 2. SP momentum is greater than that of free-space photon ($k_{sp} > k_0\sqrt{\varepsilon_d}$), i.e. light in the form of plane wave is not able to excite SPs. In this system, we have an LHM medium (Layer 2) on top of a metal layer (Layer 1) with permittivity and permeability, (ε_2, μ_2) and (ε_1, μ_1), respectively

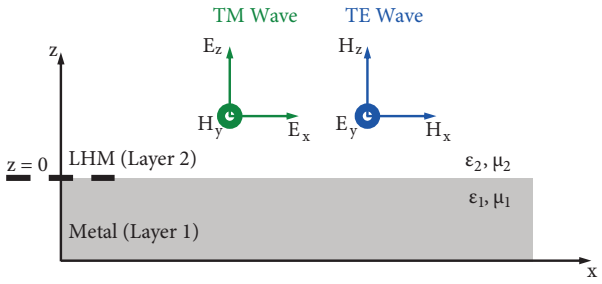

Figure 2. TM- and TE-polarized evanescent waves impinging on a two-layer medium, consisting of an LHM and a metal layer.

We first investigated a TM-polarized evanescent wave, propagating along x-direction and decaying along z-direction as schematically shown in Figure 2. In Layer 2 ($z > 0$), electric and magnetic fields are:

$$H_{(2)} = \hat{y} A e^{-jk_x^{(2)}x - k_z^{(2)}z + j\omega t},$$

$$E_{(2)} = \left(\frac{A}{j\omega\varepsilon_0\varepsilon_{(2)}}\right)(\hat{x}k_z^{(2)} - \hat{z}jk_z^{(2)}) e^{-jk_x^{(2)}x - k_z^{(2)}z + j\omega t}.$$

In Layer 1 ($z < 0$),

$$H_{(1)} = \hat{y} B e^{-jk_x^{(1)}x + k_z^{(1)}z + j\omega t},$$

$$E_{(1)} = \left(-\frac{B}{j\omega\varepsilon_0\varepsilon_{(1)}}\right)(\hat{x}k_z^{(1)} + \hat{z}jk_z^{(1)}) e^{-jk_x^{(1)}x + k_z^{(1)}z + j\omega t},$$

where $k_z^{(1,2)}$ determines the decay in the electromagnetic fields in Layers 1 and 2, which could be determined from the Maxwell's equations:

$$\nabla^2 H - \frac{\mu_r\varepsilon_r}{c^2}\frac{\partial^2 H}{\partial t^2} = 0.$$

Inserting $H_{(1)}$ and $H_{(2)}$, we have two conditions:

$$-(k_x^{(2)})^2 + (k_z^{(2)})^2 + \left(\frac{\omega}{c}\right)^2 \mu_{(2)}\varepsilon_{(2)} = 0,$$

$$-(k_x^{(1)})^2 + (k_z^{(1)})^2 + \left(\frac{\omega}{c}\right)^2 \mu_{(1)}\varepsilon_{(1)} = 0.$$

Assuming there is no charge and current source ($\boldsymbol{J_s = 0}$ and $\boldsymbol{\rho_s = 0}$) in the system, boundary conditions, implying the fact that the tangential components of electric and magnetic fields ($\boldsymbol{x}$- and $\boldsymbol{y}$-components) at the interface should be continuous, yields:

$$\boldsymbol{A=B} \quad \boldsymbol{A\frac{k_z^{(2)}}{\varepsilon_{(2)}} = -B\frac{k_z^{(1)}}{\varepsilon_{(1)}}} \quad \rightarrow \quad \boldsymbol{\frac{k_z^{(1)}}{k_z^{(2)}} = -\frac{\varepsilon_{(1)}}{\varepsilon_{(2)}}} \ .$$

Using the relationship between $\boldsymbol{k_x}$ and $\boldsymbol{k_z}$, SP dispersion wavenumber ($\boldsymbol{k_{sp}=k_x^{(1,2)}}$) for the TM-polarized incident wave is found as:

$$\boldsymbol{k_{sp}=\frac{\omega}{c}\sqrt{\frac{\varepsilon_{(2)}\varepsilon_{(1)}\left(\varepsilon_{(1)}\mu_{(2)}-\varepsilon_{(2)}\mu_{(1)}\right)}{\left(\varepsilon_{(1)}^2-\varepsilon_{(2)}^2\right)}}}.$$

For a TE-polarized light source, in Layer 2 ($\boldsymbol{z > 0}$), electric and magnetic fields are:

$$\boldsymbol{E_{(2)}=\hat{y}Ae^{-jk_x^{(2)}x-k_z^{(2)}z+j\omega t}},$$

$$\boldsymbol{H_{(2)}=\left(-\frac{A}{j\omega\mu_0\mu_{(2)}}\right)(\hat{x}k_z^{(2)}-\hat{z}jk_z^{(2)})e^{-jk_x^{(2)}x-k_z^{(2)}z+j\omega t}}.$$

In Layer 1 ($\boldsymbol{z < 0}$),

$$\boldsymbol{E_{(1)}=\hat{y}Be^{-jk_x^{(1)}x+k_z^{(1)}z+j\omega t}},$$

$$\boldsymbol{H_{(1)}=\left(-\frac{B}{j\omega\mu_0\mu_{(2)}}\right)(\hat{x}k_z^{(1)}+\hat{z}jk_z^{(1)})e^{-jk_x^{(1)}x+k_z^{(1)}z+j\omega t}}.$$

From the Maxwell's equations,

$$\boldsymbol{\nabla^2 E-\frac{\mu_r\varepsilon_r}{c^2}\frac{\partial^2 E}{\partial t^2}=0}.$$

Inserting $\boldsymbol{H_{(1)}}$ and $\boldsymbol{H_{(2)}}$, we have two conditions:

$$\boldsymbol{-\left(k_x^{(2)}\right)^2+\left(k_z^{(2)}\right)^2+\left(\frac{\omega}{c}\right)^2\mu_{(2)}\varepsilon_{(2)}=0},$$

$$\boldsymbol{-\left(k_x^{(1)}\right)^2+\left(k_z^{(1)}\right)^2+\left(\frac{\omega}{c}\right)^2\mu_{(1)}\varepsilon_{(1)}=0}.$$

Assuming again there is no charge and current source ($\boldsymbol{J_s = 0}$ and $\boldsymbol{\rho_s = 0}$) in the system, applying the same boundary conditions yields:

$$\boldsymbol{A=B} \quad \boldsymbol{A\frac{k_z^{(2)}}{\mu_{(2)}}=B\frac{k_z^{(1)}}{\mu_{(1)}}} \quad \rightarrow \quad \boldsymbol{\frac{k_z^{(1)}}{k_z^{(2)}}=\frac{\mu_{(1)}}{\mu_{(2)}}} \ .$$

Using the relationship between $\boldsymbol{k_x}$ and $\boldsymbol{k_z}$, SP dispersion wavenumber ($\boldsymbol{k_{sp}=k_x^{(1,2)}}$) for TE-polarized incident wave is found as:

$$\boldsymbol{k_{sp}=\frac{\omega}{c}\sqrt{\frac{\mu_{(2)}\mu_{(1)}\left(\varepsilon_{(2)}\mu_{(1)}-\varepsilon_{(1)}\mu_{(2)}\right)}{\left(\mu_{(1)}^2-\mu_{(2)}^2\right)}}}.$$

In Figure 3, we compared the tangential component of the wavevector on the metal surface, $\boldsymbol{k_x^{(1)} = k_{(1)}\sin\theta}$ with SP wavevector, $\boldsymbol{k_{sp}}$. For the TM-polarized light source (Figure 3, top), $\boldsymbol{k_x}$ (black curve) is always smaller

than k_{sp} (red line), implying that for the LHM–metal configuration, TM-polarized wave is not able to excite SPs. On the other hand, for the TE-polarized wave (Figure 3, bottom), k_x starts to exceed k_{sp} at the critical angle, θ_c, shown with a green arrow (see Supporting Information text for the definition of the critical angle), i.e. TE-polarized incident light source impinging on the surface with an angle of incidence greater than the critical angle can excite SPs. This phenomenon is in contrast with the classical systems consisting of a dielectric instead of an LHM medium, where only TM-polarized wave excites SPs [23].

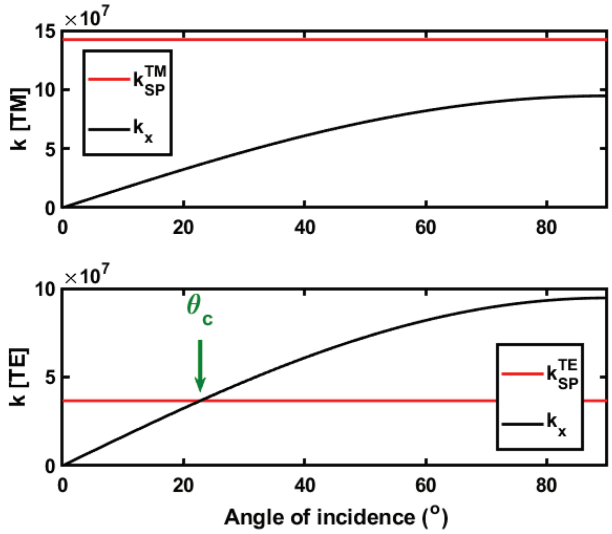

Figure 3. Tangential components of the wavevectors of (top) TM- and (bottom) TE-polarized waves (black curves) and SP wavevector (red line) for a two-layer configuration composed of an LHM and a metal layer. Calculations are performed at $\lambda = 633\,nm$, where $\varepsilon_{LHM} = -839$, $\mu_{LHM} = -977$, $\varepsilon_m = -116 - j12$, and $\mu_m = 1$.

3.2. SP excitation via Kretschmann geometry utilizing an LHM medium

In this section, we studied a three-layer Kretschmann geometry consisting of an LHM interlayer (Layer 1: $\varepsilon_{(1)}$, $\mu_{(1)}$) between a dielectric (Layer 2: $\varepsilon_{(2)}$, $\mu_{(2)}$) and a metal film (Layer 0: $\varepsilon_{(0)}$, $\mu_{(0)}$) as illustrated in Figure 4a. Here, a TE-polarized wave propagating at an angle greater than the critical angle (defined between Layers 1 and 2), excites an evanescent field in the LHM medium. This evanescent field, overcoming the momentum mismatch, excites SPs on the metal surface [8,24]. In the LHM medium, electric and magnetic fields form a left-handed orthogonal set. In this system, the main difference from the classical scheme is the direction of the waves entering the medium right after the LHM layer. As shown in Figure 4b, due to the reverse nature of the incident light source, the direction of the SPs excited at the metal surface is opposite to that of the one excited by a standard dielectric–metal system.

The electric field in Layer 2 can be written as:

$$E_{(2)} = \hat{y} e^{-jk_x^{(2)} x} \left(A_{(2)} e^{jk_z^{(2)} z} + B_{(2)} e^{-jk_z^{(2)} z} \right),$$

where $B_{(2)}$ is the amplitude of the wave, which is the sum of multiple reflections from the interface between Layers 1 and 2, as shown in Figure 4b. Here, we define a generalized reflection coefficient, [25] which is the ratio between the reflected lights in Layer 2 and the amplitude of the incident wave, i.e. $\tilde{R}_{2,1} = B_{(2)}/A_{(2)}$. Then,

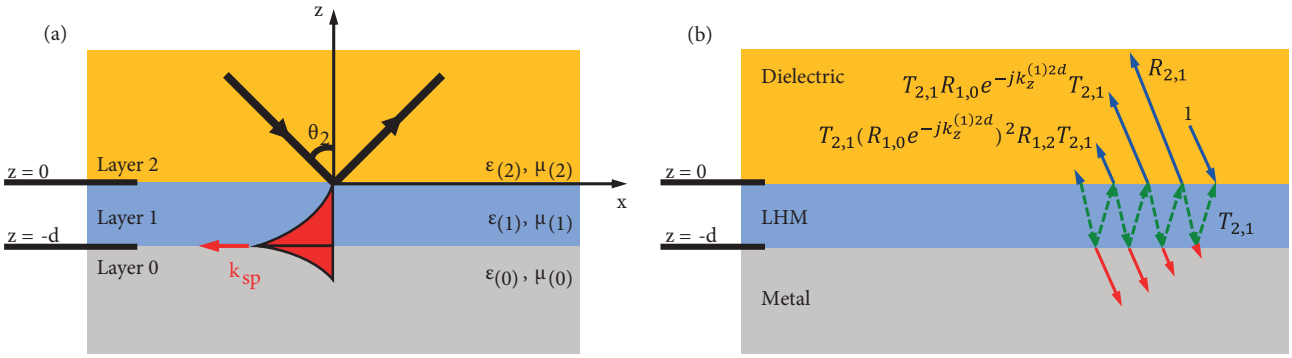

Figure 4. (a) Three-layer system exciting SPs via an LHM medium. (b) Multiple reflections and transmissions between different layers in the Kretschmann configuration utilizing an LHM interlayer.

the electric field in Layer 2 can be written as:

$$\boldsymbol{E_{(2)}}=\hat{y}\boldsymbol{A_{(2)}}e^{-j\boldsymbol{k_x^{(2)}x}}(e^{j\boldsymbol{k_z^{(2)}z}}+\tilde{R}_{\boldsymbol{2,1}}e^{-j\boldsymbol{k_z^{(2)}z}}).$$

The electric field in the LHM layer is written as:

$$\boldsymbol{E_{(1)}}=\hat{y}\boldsymbol{A_{(1)}}e^{-j\boldsymbol{k_x^{(1)}x}}(e^{j\boldsymbol{k_z^{(1)}z}}+\boldsymbol{R_{1,0}}e^{-j\boldsymbol{k_z^{(1)}(z+2d)}}).$$

The amplitude transfer between Layers 2 and 1 for the down-going waves can be written as:

$$\boldsymbol{A_{(1)}}=\boldsymbol{A_{(2)}}\boldsymbol{T_{2,1}}+\boldsymbol{A_{(1)}}\boldsymbol{R_{1,0}}e^{-j\boldsymbol{k_z^{(1)}2d}}\boldsymbol{R_{1,2}}.$$

Rearranging the terms, amplitude $\boldsymbol{A_{(1)}}$ can be written in terms of $\boldsymbol{A_{(2)}}$ as:

$$\boldsymbol{A_{(1)}}=\boldsymbol{A_{(2)}}\frac{\boldsymbol{T_{2,1}}}{\boldsymbol{1-R_{1,0}R_{1,2}}e^{-j\boldsymbol{k_z^{(1)}2d}}}.$$

The amplitude transfer between Layers 2 and 1 for the up-going waves can be written as:

$$\boldsymbol{A_{(2)}}\tilde{R}_{\boldsymbol{2,1}}=\boldsymbol{A_{(2)}}\boldsymbol{R_{2,1}}+\boldsymbol{A_{(1)}}\boldsymbol{R_{1,0}}e^{-j\boldsymbol{k_z^{(1)}2d}}\boldsymbol{T_{1,2}}.$$

Using the relationship between $\boldsymbol{A_{(1)}}$ and $\boldsymbol{A_{(2)}}$, the generalized reflection coefficient, $\tilde{R}_{\boldsymbol{2,1}}$, between Layers 1 and 2 is found as:

$$\tilde{R}_{\boldsymbol{2,1}}=\boldsymbol{R_{2,1}}+\frac{\boldsymbol{T_{1,2}T_{2,1}R_{1,0}}e^{-j\boldsymbol{k_z^{(1)}2d}}}{\boldsymbol{1-R_{1,0}R_{1,2}}e^{-j\boldsymbol{k_z^{(1)}2d}}},$$

where reflection ($\boldsymbol{R_{i+1,i}}$) and transmission ($\boldsymbol{T_{i+1,i}}$) coefficients are (see Supporting Information text for details):

$$\boldsymbol{R_{i+1,i}}=\frac{\sqrt{\boldsymbol{\varepsilon_{i+1}}}\cos\boldsymbol{\theta_i}-\sqrt{\boldsymbol{\varepsilon_i}}\sqrt{1-\frac{\boldsymbol{\varepsilon_{i+1}}}{\boldsymbol{\varepsilon_i}}\sin^2\boldsymbol{\theta_i}}}{\sqrt{\boldsymbol{\varepsilon_{i+1}}}\cos\boldsymbol{\theta_i}+\sqrt{\boldsymbol{\varepsilon_i}}\sqrt{1-\frac{\boldsymbol{\varepsilon_{i+1}}}{\boldsymbol{\varepsilon_i}}\sin^2\boldsymbol{\theta_i}}} \quad \boldsymbol{T_{i+1,i}}=\boldsymbol{1}+\boldsymbol{R_{i+1,i}}\ .$$

For the incidence angle greater than $\boldsymbol{\theta_c}$, $\sin\boldsymbol{\theta_c}=\sqrt{\boldsymbol{\mu_1\varepsilon_1}}/\boldsymbol{\mu_2\varepsilon_2}$ (see Supporting Information text for the derivation of the critical angle):

$$\boldsymbol{R_{i+1,i}}=\frac{\cos\boldsymbol{\theta_i}-\boldsymbol{j}\sqrt{\sin^2\boldsymbol{\theta_i}-\frac{\boldsymbol{\varepsilon_i}}{\boldsymbol{\varepsilon_{i+1}}}}}{\cos\boldsymbol{\theta_i}+\boldsymbol{j}\sqrt{\sin^2\boldsymbol{\theta_i}-\frac{\boldsymbol{\varepsilon_i}}{\boldsymbol{\varepsilon_{i+1}}}}}.$$

Figure 5a shows the FEM simulation of the three-layer configuration, where the incident wave is propagating with an angle greater than the critical angle (defined for the interface between the dielectric and LHM layers), showing the steady-state electric field distribution in each layer. Figure 5b shows the electric field amplitude along the propagation direction ($\boldsymbol{z}$). Surface waves propagate on any surface while they are evanescent along the directions normal to it. In our system, the wave along the interface between LHM and metal layers decays both along $+\boldsymbol{z}$ and $-\boldsymbol{z}$ directions, exhibiting its surface wave characteristics.

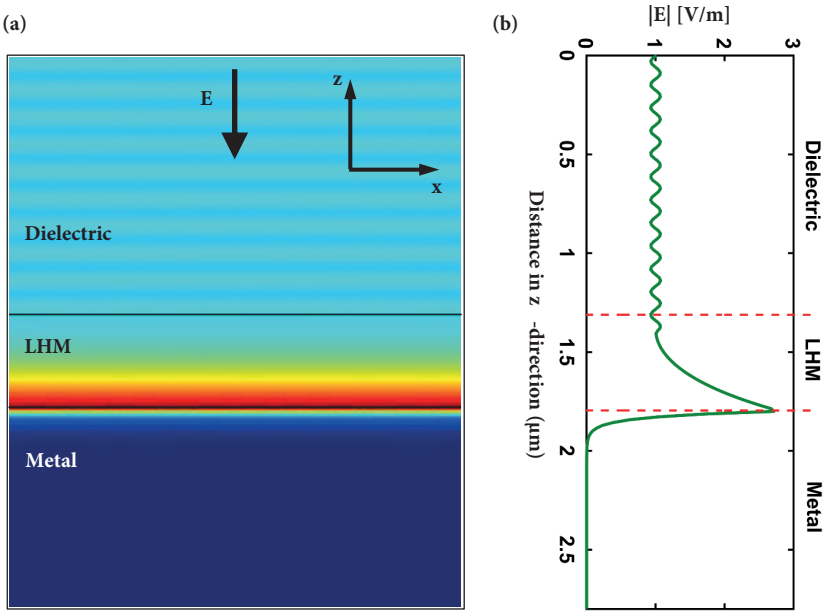

Figure 5. (a) FEM simulation of the three-layer system, which consists of a dielectric, an LHM, and a metal layer, showing the steady-state distribution of the electric field amplitude. The incident wave in the dielectric medium is propagating with an incident angle of 16.2°, where the reflectivity of the system is minimum. (b) Electric field distribution as a function of distance along the $\boldsymbol{y}$-direction (propagation direction). Corresponding device parameters are $\boldsymbol{\varepsilon_{(2)}=4}$, $\boldsymbol{\mu_{(2)}=2}$, $\boldsymbol{\varepsilon_{(1)}=-43}$, $\boldsymbol{\mu_{(1)}=-01075}$, $\boldsymbol{\varepsilon_{(0)}=-11-j12}$, $\boldsymbol{\mu_{(0)}=1}$, the wavelength of the incident light is 633 nm and the thickness of the LHM layer is 400 nm. Thicknesses of dielectric and metal layer are assumed to be infinite. In the figure, the direction of the electric field is also shown.

In Figure 6, we compared the calculated generalized reflection coefficient, $\tilde{R}_{\boldsymbol{2,1}}$ (red dashed line) and the reflection amplitude determined from FEM simulation (green line). In the FEM simulation, reflection is calculated by fitting a sum of exponentials in the GPOF method, i.e. $\boldsymbol{E=Ae^{-jkz}+Be^{+jkz}}$, where $\tilde{R}_{\boldsymbol{2,1}}=\boldsymbol{B/A}$. As shown in the figure, the calculated and simulation results coincide excellently with each other.

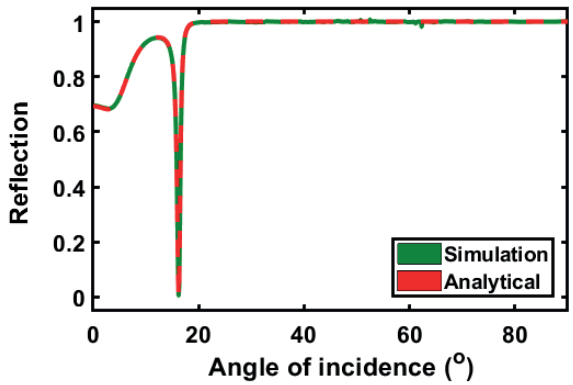

Figure 6. Generalized reflection coefficient (red dashed line) and the reflection extracted by the GPOF method from the FEM simulation (green line) for the three-layer configuration, consisting of a dielectric, an LHM, and a metal layer. Corresponding device parameters are $\varepsilon_{(2)} = 4$, $\mu_{(2)} = 2$, $\varepsilon_{(1)} = -43$, $\mu_{(1)} = -01075$, $\varepsilon_{(0)} = -11 - j12$, $\mu_{(0)} = 1$, the wavelength of the incident wave is 633 nm and the thickness of the LHM layer is 400 nm.

3.3. Effect of the LHM medium on SP propagation length

SP propagation length (L_{sp}) is the distance SPs travel until their intensity diminishes by the factor of e^2. It is calculated by taking the imaginary part of SP wavevector (the part corresponding to the energy dissipation) [26].

$$L_{sp} = \frac{1}{2k''_{sp}}.$$

For the system consisting of an LHM and a metal layer, SP wavevector becomes $k_{sp} = (\omega/c)\sqrt{\mu_2(\varepsilon_1\mu_2 - \varepsilon_2)}\Big/(\mu_{(2)}^2 - 1)$, where ε_2 and ε_1 (μ_2 and $\mu_1 = 1$) are permittivity (permeability) of the LHM and metal layers, respectively. SP propagation length is the upper limit for the subwavelength photonic devices, employing plasmonic components. For the two-layer configuration depicted in Figure 2, we used permittivity and permeability functions shown below:

$$\varepsilon_{(2)} = 1 - \frac{\omega_{pL}^2}{\omega - j\gamma},$$

$$\mu_{(2)} = 1 - \frac{F\omega_0^2}{\omega^2 - \omega_0^2 - j\Gamma_L\omega},$$

where ω_{pL} is the LHM plasma frequency (frequency of the bulk longitudinal electron excitations), γ is the damping parameter, F is a parameter between 0 and 1, Γ_L is the scattering rate (parameter showing the dissipation of electron motion), and ω_0 is the frequency at which effective permeability diverges. The frequency-dependent permittivity of the metal is determined by the Drude model:

$$\varepsilon_{(1)} = 1 - \frac{\omega_p^2}{\omega^2 - j\Gamma\omega},$$

where ω_p is the plasma frequency of the metal and Γ is the scattering rate.

Figure 7 shows the real (green line) and imaginary (red line) parts of the permittivity and permeability of the LHM and metal layers, demonstrating that when the LHM layer has negative permittivity and permeability, SP propagation length increases (blue line). This could be explained by the enhancement in the excitation of the evanescent field along the medium above the metal layer, creating stronger surface waves that can propagate longer distances before their energy dissipates.

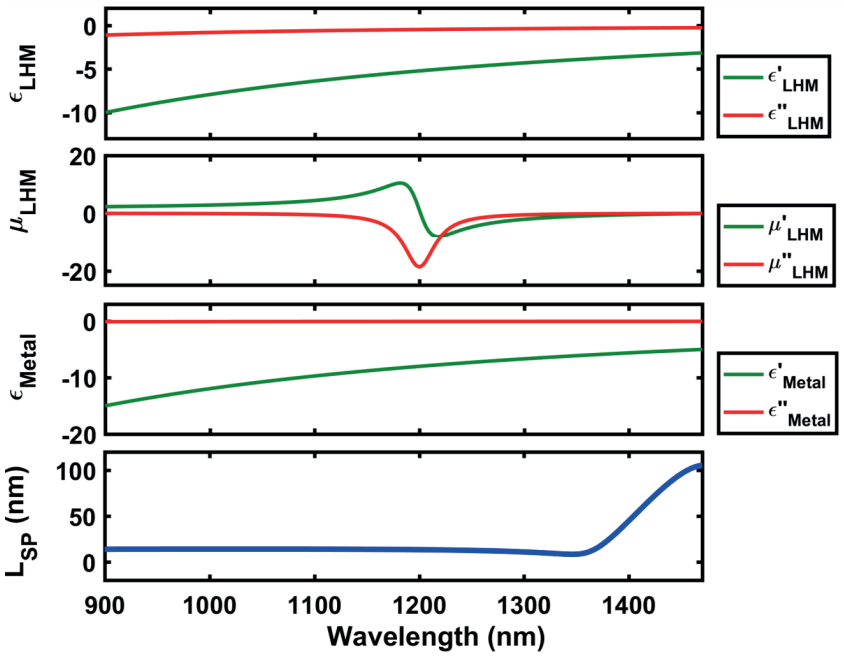

Table 7. Change in the SP propagation length with respect to the change in the permittivity ($\varepsilon_{LHM} = \varepsilon'_{LHM} - j\,\varepsilon''_{LHM}$) and permeability ($\mu_{LHM} = \mu'_{LHM} - j\,\mu''_{LHM}$) of the LHM medium and the permittivity of the metal layer ($\varepsilon_{Metal} = \varepsilon'_{Metal} - j\,\varepsilon''_{Metal}$). Corresponding device parameters are (LHM) $\omega_{pL}/2\pi = 10^{15}$ Hz (0.66 eV), $\omega_0/2\pi = 4 \times 10^{15}$ Hz (2.63 eV), $\gamma = 003\omega_{pL}$, $\Gamma_L = 003\,\omega_0$, $F = 056$ and (Metal) $\omega_p/2\pi = 12 \times 10^{15}$ Hz (7.9 eV), $\Gamma = 1.45 \times 10^{13}$ Hz (0.06 eV).

In the presence of real ($\varepsilon'_{(2)}$, $\mu'_{(2)}$) and imaginary ($\varepsilon''_{(2)}$, $\mu''_{(2)}$) parts of permittivity and the permeability, the complex wavevector in the LHM layer can be written as:

$$k_{(2)} = \frac{\omega}{c}\sqrt{n} = \frac{\omega}{c}\sqrt{\varepsilon_{(2)}\mu_{(2)}} = \frac{\omega}{c}\sqrt{(\varepsilon'_{(2)} - j\varepsilon''_{(2)})(\mu'_{(2)} - j\mu''_{(2)})}$$
$$= \frac{\omega}{c}\sqrt{(\varepsilon'_{(2)}\mu'_{(2)} - \varepsilon''_{(2)}\mu''_{(2)}) - j(\varepsilon'_{(2)}\mu''_{(2)} - \varepsilon''_{(2)}\mu'_{(2)})}.$$

Figure 8 shows the imaginary parts of the wavenumber of the incident wave in LHM medium (red line) and SP wavevector (green line) excited at the interface between the LHM and the metal layers. Here, at the wavelength (denoted with a dashed black line) where the LHM medium has negative permittivity and permeability, imaginary part of the incident evanescent field becomes less lossy. This results in surface waves with wavevector of smaller imaginary parts, demonstrating the decrease in the energy dissipation rate, which helps SP propagate longer distances. Hence, the simultaneous negative permittivity and permeability of the LHM layer can excite SPs with less lossy components such that they are able to propagate longer distances.

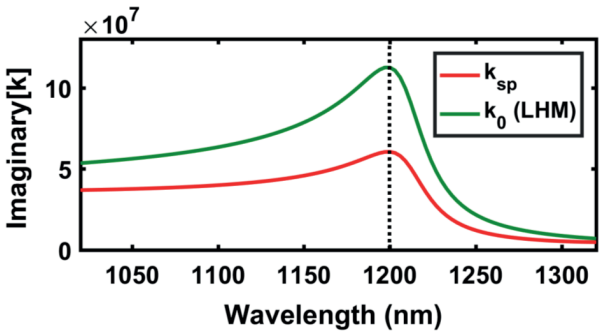

Table 8. Imaginary parts of the wavenumber of the incident wave in the LHM medium (red line) and SP wavevector (green line). Corresponding device parameters are (LHM) $\boldsymbol{\omega_{pL}/2\pi = 10^{15}}$ Hz (0.66 eV), $\boldsymbol{\omega_0/2\pi = 4 \times 10^{15}}$ Hz (2.63 eV), $\boldsymbol{\gamma = 003\omega_{pL}}$, $\boldsymbol{\Gamma_L = 003\ \omega_0}$, $\boldsymbol{F = 056}$ and (Metal) $\boldsymbol{\omega_p/2\pi = 12 \times 10^{15}}$ Hz (7.9 eV), $\boldsymbol{\Gamma = 1.45 \times 10^{13}}$ Hz (0.06 eV).

An ideal plasmonic platform of metallic apertures or particles could dramatically enhance the local electromagnetic fields associated with SPs by lowering the dissipation energy. SPs in periodic metallic systems could propagate longer wavelengths, constituting periodic elements that could communicate more efficiently. Experimental realization of such systems, i.e. covering plasmonic surfaces with LHM media, could open doors to plasmonic platforms with strong optical responses associated with large nearfield enhancements.

4. Discussion

In conclusion, we studied the dispersion relation of SPs created along an LHM–metal interface. We investigated light polarizations enabling SP excitation through LHM platforms and showed that unlike the classical scheme, with LHM, SPs are excited through a TE-polarized incident light source. We theoretically investigated the excitation of SPs with a Kretschmann geometry utilizing an LHM interlayer between a dielectric and a metal layer through FEM simulations and GPOF calculations. We also studied the effect of LHMs on SP propagation length and showed that systems utilizing an LHM layer can excite SPs with lower energy dissipation rate, allowing longer propagation distances. This could be very advantageous for applications demanding low-loss optical components, where material losses can be compensated with the use of an LHM layer.

References

[1] Pendry, J. B.; Holden, A. J.; Robbins, D. J.; Stewart, W. J. *IEEE Trans. Microwave Theory Tech.* **1999,** *47*, 2075-2084.

[2] Shelby, R. A.; Smith, D. R.; Schultz, S. *Science* **2001,** *292*, 77-79.

[3] Hoffman, A. J.; Alekseyev, L.; Howard, S. S.; Franz, K. J.; Wasserman, D.; Podolskiy, V. A.; Narimanov, E. E.; Sivco, D. L.; Gmachl, C. *Nature Mater.* **2007,** *6*, 946-950.

[4] Marques, R.; Baena, J. D.; Martel, J.; Medina, F.; Falcone, F.; Sorolla, M.; Martin, F. In *Proceedings of the International Conference on Electromagnetic Advamced Applicatiopns, ICEAA*, Torino, Italy, 8–12 September 2003.

[5] Alu, A.; Salandrino, A.; Engheta, N. *Opt. Express.* **2006,** *14*, 1557-1567.

[6] Padilla, W. J.; Smith, D. R.; Basov, D. N. *J. Opt. Soc. Am. B.* **2006,** *23*, 404-414.

[7] Barnes, W. L.; Dereux, A.; Ebbesen, T. W. *Nature* **2003,** *424*, 824-830.

[8] Raether H. *Surface Plasmons on Smooth and Rough Surfaces and on Gratings*; Springer-Verlag: New York, NY, USA, 1988.

[9] Zayats, A. V.; Smolyaninov, I. I.; Maradudin, A. A. *Phys. Rep.* **2005,** *408*, 131-314.

[10] Henri, J.; He, Y.; Niko, G.; Zhipei, S. *Optica* **2016,** *3*, 151-158.

[11] Ebbesen, T. W.; Lezec, H. J.; Ghaemi, H. F.; Thio, T.; Wolff, P. A. *Nature* **1998,** *391*, 667-669.

[12] Schouten, H. F.; Kuzmin, N.; Dubois, G.; Visser, T. D.; Gbur, G.; Alkemade, P. F. A.; Blok, H.; Hooft, G. W.; Lenstra, D.; Eliel, E. R. *Phys. Rev. Lett.* **2005,** *94*, 053901.

[13] Zhang, H. F.; Wang, Q.; Shen, N. H.; Li, R.; Chen, J.; Ding, J.; Wang, H. T. *J. Opt. Soc. Am. B* **2005,** *22*, 2686-2696.

[14] Tao, F.; Zhang, H. F.; Yang, X. H.; Cao, D. *J. Opt. Soc. Am. B* **2009,** *26,* 50-59.

[15] Ishimaru, A.; Jaruwatanadilok, S.; Kuga, Y. *Prog. Electromagn. Res.* **2005,** *51*, 139-152.

[16] Ruppin, R. *J. Phys. Condens. Matter.* **2001,** *13*, 1811-1891.

[17] Ruppin, R. *Phys. Lett. A.* **2000,** *277*, 61-64.

[18] Shadrivov, I. V.; Sukhorukov, A. A.; Kivshar, Y. S. *Phys. Rev. E.* **2004,** *69*, 016617.

[19] Hua, Y.; Sarkar, T.K. *IEEE Trans. Antennas Propag.* **1989,** *37*, 229-234.

[20] Aksun, M. I.; Alparslan, A.; Karabulut, E. P.; Irci, E.; Ertürk, V. B. *IEEE Trans. Microw. Theory Tech.* **2008,** *56*, 1423-1434.

[21] Dural, G.; Aksun, M. I. *IEEE Trans. Microw. Theory Tech.* **1995,** *43*, 1545-1552.

[22] Veselago, V.; Braginsky, L.; Shklover, V.; Hafner, C. *J. Comput. Theor. Nanosci.* **2006,** *3*, 1-30.

[23] Pitarke, J. M.; Silkin, V. M.; Chulkov, E. V.; Echenique, P. M. *Rep. Prog. Phys.* **2006,** *70*, 1-87.

[24] Moreno, L. M.; Garcia-Vidal, F. J.; Lezec, H. J.; Pellerin, K. M.; Thio, T.; Pendry, J. B.; Ebbesen, T. W. *Phys. Rev. Lett.* **2001,** *86*, 1114-1117.

[25] Chew, W. C. *Waves and Fields in Inhomogeneous Media.* IEEE Press: New York, NY, USA, 1995.

[26] Zayats, A. V.; Smolyaninov, I. I.; Maradudin, A.A. *Phys. Rep.* **2004,** *408*, 131-314.

SUPPORTING INFORMATION

Generalized pencil of function (GPOF) method

GPOF is a linear method to approximate functions by sum of complex exponentials. It consists of two steps, (i) solving the matrix equation, and (ii) finding the roots of polynomials. Electromagnetic signals can be approximated as:

$$y(t) = \sum_{i=1}^{M} R_i e^{s_i t} \quad 0 \le t \le T,$$

where R_i is the residue, s_i is the complex pole of the signal ($s_i = -\alpha_i + j\omega_i$), α_i is the damping factor, and ω_i is the angular frequency ($\omega_i = 2\pi f_i$).

After sampling the data with the sampling period, electromagnetic signal approximation can be written as:

$$y(kT_s) = \sum_{i=1}^{M} R_i {z_i}^k \quad k = 0, \dots, N-1,$$

where z_i is the complex pole in the Z domain, $z_i = e^{s_i T_s} = e^{(-\alpha_i + j\omega_i)T_s}$, $i = 1, \dots, M$. After sampling, the problem turns into finding the optimum values of M, R, and s from the sampled signal $y(kT_s)$. In the GPOF method, z_i is found as the solution of the generalized eigenvalue problem. The GPOF method extracts the poles from an exponentially damped sinusoid and treats the pole extraction as a general eigen-analysis problem. For the following set of information vectors, $\bar{y}_0, \bar{y}_1, \dots, \bar{y}_L$:

$$\bar{y}_i = [y_i, y_{i+1}, \dots, y_{i+N-L-1}]'.$$

Considering a data matric of noisy data, i.e. $[Y] = [\bar{y}_0, \bar{y}_1, \dots, \bar{y}_L]$, in the GPOF method, the information matrix is divided into two matrices in order to determine the eigenvalues of the system. Defining two matrices with sizes $(N-L)\times L$, $[Y_1]$ and $[Y_2]$:

$$[Y_1] = [\bar{y}_0, \bar{y}_1, \dots, \bar{y}_{L-1}], \quad [Y_2] = [\bar{y}_1, \bar{y}_2, \dots, \bar{y}_{L-1}].$$

Hence, the matrices can be written as:

$$[Y] = \begin{bmatrix} y(0) & y(1) & \dots & y(L) \\ y(1) & y(2) & \dots & y(L+1) \\ \vdots & \vdots & \vdots & \vdots \\ y(N-L-1) & y(N-L) & \dots & y(N-1) \end{bmatrix}_{(N-L)\times(L+1)},$$

$$[Y_1] = \begin{bmatrix} y(0) & y(1) & \dots & y(L-1) \\ y(1) & y(2) & \dots & y(L) \\ \vdots & \vdots & \vdots & \vdots \\ y(N-L-1) & y(N-L) & \dots & y(N-2) \end{bmatrix}_{(N-L)\times L},$$

$$[Y_2] = \begin{bmatrix} y(1) & y(2) & \dots & y(L) \\ y(2) & y(3) & \dots & y(L+1) \\ \vdots & \vdots & \vdots & \vdots \\ y(N-L) & y(N-L+1) & \dots & y(N-1) \end{bmatrix}_{(N-L)\times L}.$$

We first define an error measurement system which gets the information of the system by checking and comparing the data of input $u(t)$ and output $y(t)$. We can then describe the time response of the system as:

$$h(t) = \sum_{i=1}^{n} A_i e^{\lambda_i t},$$

where λ_i is the pole of the system. Then, the convolution of the system with noise $q(t)$ can be written as:

$$y(t) = h(t) * [u(t) + q(t)] = \sum_{i=1}^{n} e^{\lambda_i t} A_i \int_0^t e^{-\lambda_i \tau}[u(\tau) + q(\tau)]d\tau.$$

The set of pencil is then:

$$y_1(t) - \lambda y_2(t), \dots, y_n(t) - \lambda y_{n+1}(t); u_2(t), \dots, u_{n+1}(t),$$

and they are independent if λ becomes one of the system poles.

When the noise of the data is ignored, the information data is written as:

$$y(t) = \sum_{i=1}^{n} e^{\lambda_i t} A_i \int_0^t e^{-\lambda_i \tau} u(\tau)d\tau.$$

The output of the system is:

$$y(t) = \sum_{j=1}^{n} A_j p_j(t),$$

where $p_j(t) = e^{\lambda_j t} \int_0^t e^{-\lambda_j \tau} u(\tau)d\tau \quad j = 1, \dots, n$.

Considering a linear filter between input and output, we can write them as:

$$u_{i+1}(t) = \int_0^t u_i(\tau)d\tau \quad i = 1, \dots, n$$
$$y_{i+1}(t) = \int_0^t y_i(\tau)d\tau \quad i = 1, \dots, n.$$

The information data is formulated as:

$$y_{i+1}(t) = \sum_{j=1}^{n} A_j \left[\frac{p_j(t)}{\lambda_j^i} - \sum_{m=1}^{i} \frac{u_{m+1}(t)}{\lambda_j^{i-m+1}}\right] \quad i = 1, \dots, n.$$

This equation implies that the pencil sets $y_1(t) - \lambda y_2(t), \dots, y_n(t) - \lambda y_{n+1}(t)$; $u_2(t), \dots, u_{n+1}(t)$ are linearly dependent when λ takes the same value with one of the system poles as the pencil set bounds the independent set of functions, $A_1 p_1(t), \dots, A_n p_n(t)$; $u_2(t), \dots, u_{n+1}(t)$ by the $2n \times 2n$ matrix as follows:

$$\begin{bmatrix} E & X \\ 0 & I \end{bmatrix},$$

where I and 0 are the identity and zero matrices of order n. Here, the matrix assumption depends on the matrix E:

$$E = \left[e_{ij} = (1 - \lambda/\lambda_j)/\lambda_j^{i-1}\right] \quad i, j = 1, \dots, n,$$

where $M < L < N - M$, z_i becomes eigenvalue of the system of the matrix pencil $[Y_2] - z[Y_1]$. Here, the classical eigenvalue problem is defined as the solution of $[A]v_n = \lambda_n v_n$, $n = 1, \dots, M$, where λ is the eigenvalue and v_n is the eigenvector of the matrix $[A]$.

Two matrices $[Y_1]$ and $[Y_2]$ can be described as:

$$[Y_2] = [Z_1][R][Z_0][Z_2], \quad [Y_1] = [Z_1][R][Z_2],$$

where

$$[Z_1] = \begin{bmatrix} 1 & 1 & \dots & 1 \\ z_1 & z_2 & \dots & z_M \\ \vdots & \vdots & \vdots & \vdots \\ z_1^{N-L-1} & z_2^{N-L-1} & \dots & z_M^{N-L-1} \end{bmatrix}_{(N-L)\times M},$$

$$[Z_2] = \begin{bmatrix} 1 & z_1 & \dots & z_1^{L-1} \\ 1 & z_2 & \dots & z_2^{L-1} \\ \vdots & \vdots & \vdots & \vdots \\ 1 & z_M & \dots & z_M^{L-1} \end{bmatrix}_{M \times L},$$

$$[Z_0] = diag[z_1, z_2, \dots, z_M],$$

$$[R] = diag[R_1, R_2, \dots, R_M].$$

The pencil matrix equation becomes $[Y_2] - \lambda[Y_1] = [Z_1][R]([Z_0] - \lambda[I])[Z_2]$. When $\lambda = z_i$ ($i = 1,2, \dots, M$), i^{th} row of $[Z_0] - \lambda[I]$ becomes zero and its rank becomes $M - 1$. When $[Z_0] - \lambda[I]$ is zero, two matrices, $[Z_1]$ and $[Z_2]$ vanishes. Hence, z_i is found as the generalized eigenvalue of the matrix pair ($[Y_2]$; $[Y_1]$). The problem then turns into finding the eigenvalues of the matrix pencil problem. We first write the convolution matrix ($[]^+$ denotes pseudo-inverse):

$$\begin{aligned} [Y_1]^+[Y_2] &= [Z_2]^+[R]^{-1}[Z_1]^+[Z_1][R][Z_0][Z_2] \\ &= [Z_2]^+[Z_0][Z_2] \end{aligned}.$$

Using the vector, $\bar{p}_i$ ($= [p_i, p_{i+1}, \dots, p_{i+N-L}]^T$), and the generalized eigenvector of $[Y_1]$-$z[Y_2]$

$$\begin{aligned} [Y_1]^+[Y_1]\bar{p}_i &= \bar{p}_i \quad i = 1, \dots, M \\ [Y_1]^+[Y_2]\bar{p}_i &= z_i\bar{p}_i \quad i = 1, \dots, M \end{aligned}.$$

Then, we calculate the pseudo inverse using the singular value decomposition of $[Y_1]$:

$$\begin{aligned} [Y_1] &= \sum_{i=1,M} s_i\bar{u}_i\bar{v}_i^H = [U][S][V]^H \\ [Y_1]^+ &= [V][S]^{-1}[U]^H \end{aligned},$$

where $[U] = [\bar{u}_1, \dots, \bar{u}_M]$ is the matrix containing the left singular vectors of $[Y_1]$, $[V] = [\bar{v}_1, \dots, \bar{v}_M]$ is the matrix containing the right singular vectors of $[Y_1]$, and $[S] = diag[s_1, \dots., s_M]$ ($[]^H$ denotes the conjugate transpose of a matrix).

When the data $y(t)$ is noisy, we choose the singular values, $s_1, \dots., s_M$, to be the M largest values of $[Y_1]$ ($[Y_1]^+$ is the truncated pseudo inverse of $[Y_1]$). Now, $[Y_1]^+ - [Y_1]$ multiplied by $[V]^H$ yields:

$$([Z] - z_i[I])\bar{z}_i = 0 \quad i = 1, \dots, M,$$

where $[Z] = [S]^{-1}[U]^H[Y_2][V]$ and $\bar{z}_i = [V]^H\bar{p}_i$. $[Z]$ is an $M \times M$ matrix, z_i and $\bar{z}_i$ are eigenvalue and eigen vector of $[Z]$, respectively. The optimal choice of M can be done with the following procedure. The SVD of $[Y]$ is $[Y] = [U][S][V]^H$, where $[U]$ and $[V]$ are unitary matrices composed of eigenvectors of $[Y][Y]^H$ and $[Y]^H[Y]$, respectively and $[S]$ is the diagonal matrix composed of the singular values of $[Y]$, i.e. $[U]^H[Y][V] = [S]$.

After finding the singular values of $[Y]$, we start to compare the ratio of different singular values. We define a singular value s_c, i.e. $s_c/s_{max} \approx 10^{-p}$, where p is the number of significant decimal digits in the data. For the ratio of the singular values lower than 10^{-n}, singular values are noisy and cannot be used to reconstruct the data. $[V']$ is the filtered matrix which is constructed after selecting the value, M, and filtering the data, so it contains only M dominant right singular vectors of $[V]$.

$$[V'] = [v_1, v_2, \dots, v_M].$$

The two matrices, $[Y_1]$ and $[Y_2]$ turn into:

$$[Y_1] = [U][S'][V'_1]^H,$$

$$[Y_2] = [U][S'][V'_2]^H,$$

where $[S']$ is obtained from the M columns of $[S]$ corresponding to the M dominant singular values. Thus, the eigenvalues of the following matrix for the noiseless matrix, $[Y]$:

$$([Y_2] - \lambda[Y_1])_{L\times M} \rightarrow ([Y_1]^+[Y_2] - \lambda[I])_{M\times M}$$

are equivalent to the eigenvalues of the matrix below:

$$([V'_2] - \lambda[V'_1]^H) \rightarrow ([V'_1]^H)^+([V'_2]^H)^+ - \lambda[I].$$

The algorithm provides the minimum variance when estimating z_i in the presence of noise. After finding M and z_i, R_i can be found from the following matrix solution:

$$\begin{bmatrix} y(0) \\ y(1) \\ \vdots \\ y(N-1) \end{bmatrix} = \begin{bmatrix} 1 & 1 & \dots & 1 \\ z_1 & z_2 & \dots & z_M \\ \vdots & \vdots & \vdots & \vdots \\ z_1^{N-L-1} & z_2^{N-L-1} & \dots & z_M^{N-L-1} \end{bmatrix} \begin{bmatrix} R_1 \\ R_2 \\ \vdots \\ R_M \end{bmatrix}$$

Critical angle between two dielectric layers

For an incident wave travelling between two media, it obeys the Snell's law, i.e. $\sqrt{\varepsilon_2\mu_2}\sin\theta_2 = \sqrt{\varepsilon_1\mu_1}\sin\theta_1$. When $\varepsilon_2 \gg \varepsilon_1$, a critical angle is defined as the angle which makes the refraction angle $\theta_1 = \pi/2$ such that no transmission exists from layer 2 to 1:

$$\theta_c = \theta_2 \Rightarrow \theta_1 = \pi/2 \Rightarrow \theta_c = \sin^{-1}\sqrt{\frac{\varepsilon_1\mu_1}{\varepsilon_2\mu_2}}.$$

Reflection coefficient of a TE-polarized wave propagating between two dielectric layers

In order to determine the reflection coefficients for the Kretschmann geometry, we utilize the three-layered system where we have multiple reflections and transmission between different layers (Figure 4b). For a TE-polarized wave propagating between two dielectric media,

$$E_{i+1} = \hat{y}\left(E_{i+1}^{+}e^{-jk_z^{(i+1)}z - jk_x^{(i+1)}x} + E_{i+1}^{-}e^{+jk_z^{(i+1)}z - jk_x^{(i+1)}x}\right),$$

$$E_i = \hat{y}\left(E_i^{+}e^{-jk_z^{(i)}z - jk_x^{(i)}x} + E_i^{-}e^{+jk_z^{(i)}z - jk_x^{(i)}x}\right),$$

defining $R_{i+1,i}$ and $T_{i+1,i}$ as the reflection and transmission coefficients of the incident wave from layer $i+1$ to i, and E_0 as the amplitude of the incident wave, then the amplitude of the electric field in each medium can be written as follows:

$$E_{i+1}^{-} = E_0, \quad E_{i+1}^{+} = R_{i+1,i}E_0, \quad E_i^{+} = 0, \quad E_i^{-} = T_{i+1,i}E_0.$$

Then the electric field in two media becomes:

$$E_{i+1} = \hat{y}E_0e^{-jk_x^{(i+1)}x}\left(e^{+jk_z^{(i+1)}z} + R_{i+1,i}e^{-jk_z^{(i+1)}z}\right),$$

$$E_i = \hat{y}T_{i+1,i}E_0 e^{-jk_x^{(i)}x} e^{+jk_z^{(i)}z}.$$

Substituting these electric field definitions to Maxwell's curl equation ($\nabla \times E = -j\omega\mu H$), magnetic fields are determined as:

$$H_{i+1} = -\frac{E_0 e^{-jk_x^{(i+1)}x}}{j\omega\mu}\left(\left[-\hat{z}jk_x^{(i+1)} - \hat{x}jk_z^{(i+1)}\right]e^{+jk_z^{(i+1)}z} + [-\hat{z}jk_x^{(i+1)} + \hat{x}jk_z^{(i+1)}]R_{i+1,i}e^{-jk_z^{(i+1)}z}\right),$$

$$H_i = -\frac{T_{i+1,i}E_0 e^{-jk_x^{(i)}x}}{j\omega\mu}(-\hat{z}jk_x^{(i)} - \hat{x}jk_z^{(i)})e^{jk_z^{(i)}z}.$$

The boundary condition, implying that the tangential components of electric and magnetic fields (x and y) are continuous, yields:

$$1 + R_{i+1,i} = T_{i+1,i} \quad k_z^{(i+1)}\left(1 - R_{i+1,i}\right) = k_z^{(i)}T_{i+1,i}.$$

Hence, the reflection coefficient of the TE-polarized wave is obtained as ($k_z = k_0\sqrt{\varepsilon}\cos\theta$):

$$R_{i+1,i} = \frac{k_z^{(i+1)} - k_z^{(i)}}{k_z^{(i+1)} + k_z^{(i)}} \longrightarrow R_{i+1,i} = \frac{k_0\sqrt{\varepsilon_{i+1}}\cos\theta_{i+1} - k_0\sqrt{\varepsilon_i}\cos\theta_i}{k_0\sqrt{\varepsilon_{i+1}}\cos\theta_{i+1} + k_0\sqrt{\varepsilon_i}\cos\theta_i}.$$

Arranging terms and using $\cos^2\theta = 1 - \sin^2\theta$:

$$R_{i+1,i} = \frac{\sqrt{\varepsilon_{i+1}}\cos\theta_{i+1} - \sqrt{\varepsilon_i}\sqrt{1 - \frac{\varepsilon_{i+1}}{\varepsilon_i}\sin^2\theta_i}}{\sqrt{\varepsilon_{i+1}}\cos\theta_{i+1} + \sqrt{\varepsilon_i}\sqrt{1 - \frac{\varepsilon_{i+1}}{\varepsilon_i}\sin^2\theta_i}}.$$

Reflection coefficient of a TE-polarized wave propagating at an angle greater than the critical angle between two dielectric layers

When the incident angle is greater than the critical angle, $\theta_c = \sin^{-1}\sqrt{\varepsilon_i/\varepsilon_{i+1}}$:

$$\sin\theta_i > \sin\theta_c = \sqrt{\frac{\varepsilon_i}{\varepsilon_{i+1}}} \rightarrow \sin\theta_{i+1} > 1.$$

The inequality is satisfied for the complex solutions of θ_{i+1}:

$$k_i = \hat{x}k_x^{(i)} - \hat{z}k_z^{(i)},$$

where

$$k_x^{(i)} = k_i \sin\theta_i,$$

$$k_z^{(i)} = k_i \cos\theta_i = k_i\sqrt{1 - \frac{\varepsilon_{i+1}}{\varepsilon_i}\sin^2\theta_i} = k_0\sqrt{\varepsilon_i}\sqrt{1 - \frac{\varepsilon_{i+1}}{\varepsilon_i}\sin^2\theta_i}$$

$$\longrightarrow k_z^{(i)} = k_0\sqrt{\varepsilon_{i+1}}\sqrt{\frac{\varepsilon_i}{\varepsilon_{i+1}} - \sin^2\theta_i} = jk_{i+1}\sqrt{\sin^2\theta_i - \frac{\varepsilon_i}{\varepsilon_{i+1}}}.$$

Then the electric and magnetic fields in each vector are written as:

$$E_{i+1} = \hat{y}E_0 e^{-jk_{i+1}\sin\theta_{i+1}x}\left(e^{+jk_{i+1}\cos\theta_{i+1}z} + R_{i+1,i}e^{-jk_{i+1}\cos\theta_{i+1}z}\right),$$

$$E_i = \hat{y}T_{i+1,i}E_0 e^{-jk_i\sin\theta_i x}e^{-k_{i+1}\sqrt{\sin^2\theta_i - \frac{\varepsilon_i}{\varepsilon_{i+1}}}},$$

$$H_{i+1} = -\frac{E_0 e^{-jk_{i+1}\sin\theta_{i+1}x}}{j\omega\mu}([-\hat{z}jk_{i+1}\sin\theta_{i+1} - \hat{x}jk_{i+1}\cos\theta_{i+1}]e^{+jk_{i+1}\cos\theta_{i+1}z} +$$

$$[-\hat{z}jk_{i+1}\sin\theta_{i+1} + \hat{x}jk_{i+1}\cos\theta_{i+1}]R_{i+1,i}e^{-jk_{i+1}\cos\theta_{i+1}z}),$$

$$H_i = -\frac{T_{i+1,i}E_0 e^{-jk_i\sin\theta_i x}}{j\omega\mu}\left(-\hat{z}jk_i\sin\theta_i + \hat{x}k_{i+1}\sqrt{\sin^2\theta_i - \frac{\varepsilon_i}{\varepsilon_{i+1}}}\right)e^{-k_{i+1}\sqrt{\sin^2\theta_i - \frac{\varepsilon_i}{\varepsilon_{i+1}}}z}.$$

Here, the field in layer i is evanescent (exciting SPs in layer $i+1$) when $\varepsilon_{i+1} \gg \varepsilon_i$ and the incident angle is greater than the critical angle defined between two layers. Using the continuous boundary conditions for both electric and magnetic fields, the reflection coefficient is calculated as:

$$R_{i+1,i} = \frac{\cos\theta_i - j\sqrt{\sin^2\theta_i - \frac{\varepsilon_i}{\varepsilon_{i+1}}}}{\cos\theta_i + j\sqrt{\sin^2\theta_i - \frac{\varepsilon_i}{\varepsilon_{i+1}}}}.$$